The Role of Precipitation Variability in Closing the Global Atmospheric Energy Budget

Alexander V. Matus[1,2], Ryan J. Kramer[3], Lazaros Oreopoulos[2], Nayeong Cho[1,2]

[1]University of Maryland Baltimore County, Baltimore, MD, USA
[2]NASA Goddard Space Flight Center, Greenbelt, MD, USA
[3]NOAA Geophysical Fluid Dynamics Laboratory, Princeton, NJ, USA

Submitting to:

Geophysical Research Letters

(2026)

Corresponding Author: amatus@umbc.edu

Highlights

1. GPCP v3.3 achieves 98% mean atmospheric energy closure, with a residual of -2.4 ± 9.5 W/m².
2. Improved mean closure, however, comes with a sharp increase in interannual variability.
3. This interannual variability is linked to enhanced precipitation in the Tropical Western Pacific.

Keywords

1. Atmospheric Energy Budget
2. Precipitation
3. Climatology
4. Radiative Cooling
5. Energy Closure
6. Interannual Variability
7. Tropical Western Pacific

Codes for AGU submission:

- 3354 (Precipitation)
- 3305 (Atmospheric energy budget)
- 1622 (Earth system modeling/Global climate models)
- 3360 (Remote sensing)

Abstract

The global hydrologic cycle is constrained by the atmospheric energy budget: net atmospheric radiation (Q_{atm}) must be balanced by latent heat flux from precipitation (LP) and sensible heat flux (SH). Historically, independent satellite observations have failed to achieve this closure, consistent with radiative-convective equilibrium, leaving a residual imbalance. We evaluate three generations of the Global Precipitation Climatology Project (GPCP v2.3, v3.2, and v3.3) alongside CERES radiation and ERA5 sensible heat flux, among other data sources. We find that GPCP v3.3 achieves a 98% mean multiannual energy closure (residual of -2.4 ± 9.5 W/m²), a significant improvement over v2.3 (residual of -13.5 ± 10.0 W/m²). However, this improved mean-state agreement is accompanied by a considerable increase in the interannual variability of the budget residual. We demonstrate that this increased variance originates from localized precipitation adjustments in the tropical Western Pacific, potentially linked to improved detection of convective extremes. This study highlights a fundamental trade-off between mean-state accuracy and anomaly stability in satellite products, providing critical context for future studies of climate variability and the evaluation of Earth System models.

1. Introduction

The global hydrological cycle is a fundamental component of the Earth's climate system. Understanding its drivers is critical for predicting water availability and managing resources in a warming world. Global moisture availability increases at approximately 7% per Kelvin according to the Clausius-Clapeyron relationship; however, global mean precipitation is constrained to a lower rate of increase of 2–3% per Kelvin (Held and Soden, 2006). This discrepancy arises because the global hydrological cycle is fundamentally limited by the atmosphere's ability to radiate away the latent heat released during condensation (Stephens et al., 2012; O'Gorman et al., 2012). Therefore, the net atmospheric radiation (Q_{atm}) serves as the primary regulator of global precipitation.

We define Q_{atm} as the difference between the net TOA radiation and net surface radiation:

$$Q_{atm} = (SW_{TOA} + LW_{TOA}) - (SW_{SFC} + LW_{SFC}) \qquad (1)$$

Under this sign convention, a positive Q_{atm} represents a net energy gain (heating) in the atmospheric column (Oreopoulos et al., 2025). On annual or longer timescales, radiative convective equilibrium (RCE) describes the balance between atmospheric cooling and heating through latent heat release and sensible heat fluxes (Jakob et al., 2019). To maintain RCE, the sum of these terms must approach zero:

$$Q_{atm} + LP + SH \approx 0 \qquad (2)$$

This vertically integrated approach provides a rigorous physical constraint for evaluating global precipitation fields (Stephens et al., 2012; L'Ecuyer et al., 2015). Theoretical and modeling studies have established that shifts in this budget, driven by greenhouse gases, aerosols, and cloud feedbacks, can profoundly alter precipitation (Allan et al., 2014; Sherwood et al., 2015). Specifically, the distribution and thermodynamic phase of clouds play a critical role in modulating these radiative cooling rates, thereby determining the energy available to be balanced by latent heating (Matus and L'Ecuyer, 2017).

While the theoretical foundation is robust, the observational evidence remains underdeveloped. Recent work has demonstrated that satellite-observed trends in Q_{atm} and P are broadly consistent (Kato et al., 2025), yet independent observational records have historically struggled to achieve absolute energy closure. This persistent residual imbalance complicates our ability to use the energy budget as a diagnostic tool for understanding the spatiotemporal variability of the water cycle. This study addresses these gaps by evaluating the energy closure across three generations of GPCP precipitation data (v2.3, v3.2, and v3.3). We investigate whether recent algorithm updates lead to improved physical reconciliation with the radiation budget and how these updates affect the interannual variability of the budget residual.

2. Datasets

2.1 Net Atmospheric Radiation

The Q_{atm} term is derived from the CERES EBAF Edition 4.2.1 product (Kato et al., 2025), which provides monthly mean radiative fluxes on a 1º×1º global grid. While TOA fluxes are based on observations by CERES instruments, surface radiative fluxes are computed using a radiative transfer model initialized with satellite-derived cloud and aerosol properties (Sun-Mack et al., 2018) and GEOS reanalysis profiles. To ensure physical consistency with observed TOA irradiance and ocean heat content, the EBAF product employs a tuning process to adjust surface and atmospheric inputs within their uncertainty ranges (Loeb et al., 2018). We also utilize estimates from ERA5 and MERRA-2 to quantify structural uncertainties in radiative cooling.

2.2 Precipitation and Sensible Heat

We compare three successive versions of the Global Precipitation Climatology Project (GPCP): legacy v2.3 (2.5º resolution), and modern v3.2 and v3.3 (0.5º resolution). While v2.3 and v3.3 extend through the end of our study period (September 2024), v3.2 is used only through April

2024 due to the ending of its operational processing. GPCP v3.3 incorporates upgraded input datasets and refined bias-correction schemes to enhance tropical precipitation accuracy (Huffman et al., 2025). Precipitation data (*P*) are converted to latent heat flux units (W/m^2) using the latent heat of vaporization ($L \approx 2.5 \times 10^6$ J/kg). Global sensible heat flux (*SH*) is obtained from the ERA5 Reanalysis (Hersbach et al., 2020), with JRA-3Q and MERRA-2 used to account for structural uncertainty in the non-radiative flux components.

2.3 GPCP Algorithm Evolution

The transition from GPCP v2.3 to the v3 series represents a fundamental shift toward the Integrated Multi-satellitE Retrievals for GPM (IMERG) framework (Huffman et al., 2020). As detailed in Table 1, GPCP v3.2 implemented IMERG to enhance detection of convective systems and light precipitation (Adler et al., 2018). The subsequent release of v3.3 resolves artifacts from v3.2, such as spatial discontinuities in high latitudes, through a more robust bias-correction framework and refined gauge-weighting logic (Huffman et al., 2025; Bolvin et al., 2024). By improving oceanic rainfall representation via the GPM Microwave Imager (GMI), v3.3 yields a latent heat flux physically consistent with CERES-observed radiative cooling (Loeb et al., 2024). While these refinements drive the 98% mean annual energy closure, the increased sensor sensitivity appears to introduce larger interannual variability in the residual.

Version	Resolution	Analysis Period	Tropical Retrieval Basis	Key Improvements for Energy Closure
v2.3	2.5º	Jan 2003 - Sep 2024	IR/PMW blend	Established multi-decadal baseline for evaluating long-term anomaly stability
v3.2	0.5º	Jan 2003 - Apr 2024	IMERG V06	Enhanced detection of tropical light rain, reducing persistent dry bias in tropics
v3.3	0.5º	Jan 2003 - Sep 2024	IMERG V07	Achieves 98% mean closure with GPM/GMI bias correction of heavy convective rain

Table 1. Characteristics of evaluated versions of GPCP datasets

3. Methods

3.1 Data Integration

To ensure physical consistency across varying native resolutions, all datasets were gridded to a common 1°×1° spatial resolution. The GPCP precipitation products and ERA5 sensible heat fluxes were collocated with the CERES grid using first-order remapping (Jones, 1999). The analysis covers January 2003 through September 2024 (truncated to April 2024 for GPCP v3.2) at a monthly temporal resolution.

3.2 Statistical Approach

When closure is expected but does not occur, the atmospheric energy residual (R) is defined as:

$$R = Q_{atm} + LP + SH \quad (3)$$

We compute deseasonalized anomalies relative to the climatology of the study period. A 12-month running mean is applied to evaluate variability at scales consistent with RCE. Uncertainty in R is assessed through formal error propagation:

$$\sigma_R = (\sigma_Q^2+\sigma_{LP}^2+\sigma_{SH}^2)^{½} \quad (4)$$

We assume a Q_{atm} uncertainty of 8.25 W/m², derived as the root-sum-square of the published CERES TOA and surface flux uncertainties (Loeb et al., 2018). The *SH* uncertainty is estimated at 1.6 W/m², representing one standard deviation across ERA5, JRA-3Q, and MERRA-2 products. Finally, we apply version-specific estimates of *LP* uncertainty: 7% for v2.3 (Adler et al., 2018), 6% for v3.2 (Huffman et al., 2023), and 5% for v3.3 (Huffman et al., 2024).

3.3 Spatial and Variability Analysis

Global maps of the mean residual and variance were generated to identify regions of energy imbalance, particularly in the Tropical Western Pacific (TWP). We analyzed the Probability Distribution Functions (PDFs) of *LP* over the TWP to determine if increased variance in v3.3 is indeed driven by improved representation of convective extremes or rather a shift in the mean precipitation state.

4. Results

4.1 Improvement in Mean-State Energy Closure

The evolution from GPCP v2.3 to v3.3 demonstrates a systematic progression toward energy budget closure. Figure 1 illustrates that the shift in mean precipitation across versions is responsible for reducing the atmospheric energy imbalance. The residual magnitude is estimated to be -13.5 ± 10.0 W/m^2 in v2.3. This residual is reduced to -10.0 ± 9.7 W/m^2 in v3.2 and further decreases to -2.4 ± 9.5 W/m^2 in v3.3. This represents 98% closure in the annual mean, placing the global imbalance well within the margin of observational uncertainty. This suggests that the algorithmic refinements in v3.3, particularly regarding tropical convective intensity, are more physically reconciled with radiation.

4.2 Shifts in Regional Precipitation Distributions

Figure 2 maps the global spatial and zonal distributions of the energy budget residual. While the global mean residual for v3.3 is near zero, significant regional deviations persist, consistent with physical expectations and with patterns identified by Jakob et al. (2019). Figure 2a reveals regional imbalances exceeding ±100 W/m^2 at low and high latitudes, respectively. These patterns underscore a persistent zonal imbalance in the observed atmospheric energy budget that is not captured by the global averages. Figure 2b shows an increase in global mean precipitation that lacked a specific regional or intensity-based focus. Figure 2c further clarifies that the notable shift toward higher residual values within the tropics in v3.3 is primarily a result of the algorithm updates implemented since the release of v3.2.

Figure 3 confirms that this improved energy closure is largely driven by increased *LP* within the tropics. The most pronounced shifts occur over the TWP (120°E–200°E, 15°S–15°N). Although the TWP covers only 6% of Earth's surface, it contributes 13% of global precipitation. As shown in Figure 3a, mean *LP* in this region increases from 81.3 W/m^2 in v3.2 to 88.9 W/m^2 in v3.3. While global-scale PDFs remain relatively stable (Figure 3b), the regional PDF for the TWP (Figure 3c) exhibits a notable rightward shift in v3.3. This is characterized by a higher frequency of high-intensity precipitation events, resulting in a localized *LP* increase of 27.6 W/m^2 in v3.3. This intensified regional precipitation appears to be the primary driver of global residual variability.

4.3 The Variability Paradox in the Time Series

While v3.3 improves mean closure, its temporal stability diverges from previous versions. Figure 4 presents a time series of global atmospheric energy budget anomalies in Q_{atm}, *LP*, *SH*, and *R* from 2003 to 2024. Figure 4a reveals that the residual anomaly, *R,* closely mirrors *LP* fluctuations, identifying precipitation as the primary driver of budget imbalances at interannual scales. Furthermore, cross-correlation analysis reveals that Q_{atm} lags *LP* by approximately 2 months. This phase lag suggests that the rapid fluctuations in the v3.3 precipitation record are not immediately compensated by radiative cooling. This likely reflects the physical timescale required for convective-core latent heating to propagate into large-scale anvil cloud radiative effects, though sensor-specific decoupling cannot be ruled out.

Figure 4b reveals that each successive GPCP version exhibits an increase in variability. Anomalies in latent heat flux have a decreasing trend in v2.3 and v3.2. However, a positive trend in v3.3 marks a sharp contrast to previous versions, which strongly influences the time series of energy budget residuals shown in Figure 4c. In a similar analysis, Kato et al. (2025) defined an uncertainty threshold of ±1.1 W/m^2, representing the square root of the sum of the variances of each atmospheric energy budget component. As described by Kato et al. (2025), the residual remaining within this envelope indicates that errors are either correlated or smaller than the individual component uncertainties. While v2.3 exceeds this bound only 4% of the time, this frequency reaches 30% in v3.3 (Figure 4c). This trend underscores a significant evolution in the GPCP dataset: while modern algorithm updates are more closely aligned with climatological energy constraints, they have introduced a greater degree of monthly variability that may impact the characterization of short term hydrological trends.

4.4 Robustness of the Radiative Constraint

To determine whether the increased residual variability originates from precipitation or from uncertainties in other energy terms, we assessed the consistency of Q_{atm} and *SH* across multiple independent datasets (Figure 5). The ensemble mean, shown in Figure 5a, reveals that anomalies in Q_{atm} and *SH* are remarkably consistent across CERES, ERA5, and MERRA-2. Even when combined, the sum of these cooling and turbulent terms exhibits high correlation ($r > 0.95$), suggesting that uncertainties in these terms are not the source of this observed interannual variability.

Statistical summaries of these anomalies (Figure 5b) further isolate precipitation as the primary driver of the variability paradox. While Q_{atm} and *SH* exhibit narrow interquartile ranges and low interannual variance, *LP* shows a progressive expansion in anomaly magnitude from legacy v2.3 to the modern v3.3 product. This growing divergence, occurring while the other budget components remain stable, reinforces the conclusion that the evolving residual behavior is a direct consequence of GPCP algorithmic updates. These results confirm that the fluctuations observed in the v3.3 global budget are not an artifact of uncertainties in Q_{atm} or *SH*, but rather a physical signal of enhanced precipitation sensitivity in the latest retrieval framework.

5. Discussion

5.1 Physical Drivers of Improved Closure

The progression toward mean-state energy closure has occurred through two distinct modes of precipitation adjustment. In contrast, the shift from v3.2 to v3.3 is physically rooted in the representation of precipitation in the TWP (Figure 3a). This latest version identifies significantly higher precipitation magnitudes within this critical convective region.

Given that the atmosphere functions as a heat engine where latent heat release must balance radiative cooling, the lower precipitation totals in previous records were a primary driver of the historical energy imbalance. The structural shift in the v3.3 PDF (Figure 3c) suggests that the current retrieval algorithms more effectively capture the high-intensity convective events required to balance the atmospheric radiative sink. This adjustment aligns the hydrological cycle with the fundamental energy constraints described by Kato et al. (2025) more closely than the broader, more uniform adjustments seen in earlier versions.

5.2 The Variability Paradox

The characteristics of these successive updates explain the discrepancy in anomaly stability across the GPCP record. Because the transition from v2.3 to v3.2 relied on a relatively uniform increase in precipitation, it did not significantly alter the interannual variance of the global residual. However, by anchoring the v3.3 improvement in high-intensity convective episodes within the Western Pacific, the algorithm has introduced a higher degree of variability.

This increased variance presents a challenge for diagnostic studies of climate variability. The apparent ENSO signal in the anomaly time series implies that the v3.3 precipitation product may be over responsive to localized convective shifts relative to the more stable global radiative constraint. While larger variance may represent a more sensitive response to ENSO driven shifts in tropical convection, the absence of a corresponding increase in the variability of the Q_{atm} record suggests a potential over response in the precipitation retrieval.

As validated by the consistency between CERES EBAF, MERRA-2, and ERA5 (Figure 5), the precipitation anomalies in v3.3 exhibit an amplified sensitivity compared to the energy sink terms. This implies that while the mean state is more accurate, the magnitude of interannual variability and the temporal decoupling in the latest precipitation product require careful consideration. Such fluctuations must not be overinterpreted as long term climate trends, as they frequently exceed the physical bounds of maintained energy balance.

5.3 Implications and Future Work

These results indicate that while the scientific community is nearing a closed loop observation of the energy and water cycles, the trade off between mean-state accuracy and anomaly stability in GPCP v3.3 necessitates a nuanced application of the data. GPCP v3.3 currently represents the most physically consistent product for climatological studies of the mean global energy budget. However, studies focused on climate signals must account for the fact that the increased variability localized in the Western Pacific may inflate the uncertainty of energy budget analyses.

This energy budget framework assumes that Q_{atm} and *SH* are stable constraints. However, shared dependencies in reanalysis temperature and humidity profiles across datasets may introduce systematic biases. The ±1.1 W/m^2 uncertainty threshold used in Section 4.3 is a global conservative estimate that does not account for the state-dependent errors inherent in tropical convective retrievals, where *LP* uncertainties are maximized. Future efforts should prioritize reconciling the interannual variability between Q_{atm} and *P*, specifically investigating the coupling between energy and precipitation during organized convective events. Ensuring that improvements in mean-state closure do not come at the expense of temporal reliability is essential for the next generation of climate monitoring products.

Conclusions

This study evaluates the evolution of global atmospheric energy budget closure across three generations of the GPCP precipitation product. Our results demonstrate that GPCP v3.3 achieves a nearly closed annual mean budget, reducing the historical energy residual from -13.5 ± 10.0 W/m^2 (v2.3) to -2.4 ± 9.5 W/m^2 (v3.3), representing a 98% closure when constrained by CERES EBAF radiative cooling and ERA5 sensible heat fluxes. This improvement is physically driven by a significant upward shift in precipitation intensity localized within the deep convective regimes of the Tropical West Pacific.

However, this transition toward mean-state accuracy reveals a significant variability paradox. While the previous update (v2.3 to v3.2) increased global precipitation through broad-scale adjustments that preserved anomaly stability, the v3.3 update focuses specifically on high-intensity convective events. This shift in the precipitation probability distribution function has introduced substantial interannual volatility into the budget. In the v3.3 record, 30% of monthly residual anomalies exceed the observational uncertainty threshold, a sevenfold increase compared to the legacy v2.3 product.

Ultimately, while GPCP v3.3 provides the most internally consistent representation of the climatological energy budget to date, its heightened sensitivity to tropical convective fluctuations necessitates caution. For researchers investigating interannual climate signals or short-term hydrological trends, the increased variability in the v3.3 record may complicate the detection of physical forced responses. Future refinements should aim to reconcile this increased precipitation variance with the relatively stable global radiative cooling record to ensure that improvements in mean-state closure do not diminish the reliability of anomaly-based climate diagnostics.

Acknowledgments

All authors were supported by NASA MEaSUREs grant 80NSSC24M0014. R.J.K. acknowledges support from the Geophysical Fluid Dynamics Laboratory (GFDL), NOAA, but the statements, findings, conclusions and recommendations are those of the author(s) and do not necessarily reflect the views of the National Oceanic and Atmospheric Administration or the US. 560 Department of Commerce. We thank Jackson Tan, David Bolvin, and Ali Behrangi for their contributions in the interpretation and analysis of GPCP precipitation data products.

Data availability statement/ Open Research

The data supporting the findings of this study are available in public repositories. Atmospheric radiative flux data from the CERES EBAF (Edition 4.2.1) were obtained from the NASA Langley Research Center Atmospheric Science Data Center (ASDC) (https://ceres.larc.nasa.gov/data/; DOI: 10.5067/TERRA+AQUA/CERES/EBAF_L3-4.2). Monthly precipitation datasets for the Global Precipitation Climatology Project (GPCP) v2.3, v3.2, and v3.3 were retrieved from the NOAA National Centers for Environmental Information (NCEI) and the NASA Goddard Earth Sciences Data and Information Services Center (GES DISC) (https://disc.gsfc.nasa.gov/). Surface sensible heat flux data from the ERA5 reanalysis were obtained from the Copernicus Climate Change Service (C3S) Climate Data Store (https://cds.climate.copernicus.eu/; DOI: 10.24381/cds.f17050d7). Radiative flux validation data from MERRA-2 were retrieved from the NASA Global Modeling and Assimilation Office via the GES DISC.

Plain Language Summary

While a warmer atmosphere can hold more moisture, the Earth's energy budget ultimately dictates the global amount of rainfall. For rain to fall, the atmosphere must release heat, primarily by radiating energy into space. This study investigates how well independent satellite observations of rainfall and atmospheric radiation align with this physical constraint. By comparing three generations of the Global Precipitation Climatology Project (GPCP) data, we found that the latest version (v3.3) brings the global water and energy cycles into much closer

agreement than previous versions, reconciling the budget to within 98%. However, we also discovered a trade-off: as the data became more accurate at representing average global rainfall, it yielded greater year-to-year changes. This increased variability is tied to how the new version tracks heavy rainfall in the tropical Western Pacific. We identified a 2-month phase lag between rainfall and the atmosphere's ability to shed heat, creating temporary non-physical imbalances in the global energy budget. Our findings suggest that while the newest precipitation records are excellent for understanding the Earth’s average state, we must be cautious when using them to study short-term climate swings. This work is a critical step toward ensuring satellite tools can accurately track changes in Earth’s atmosphere.

Figures

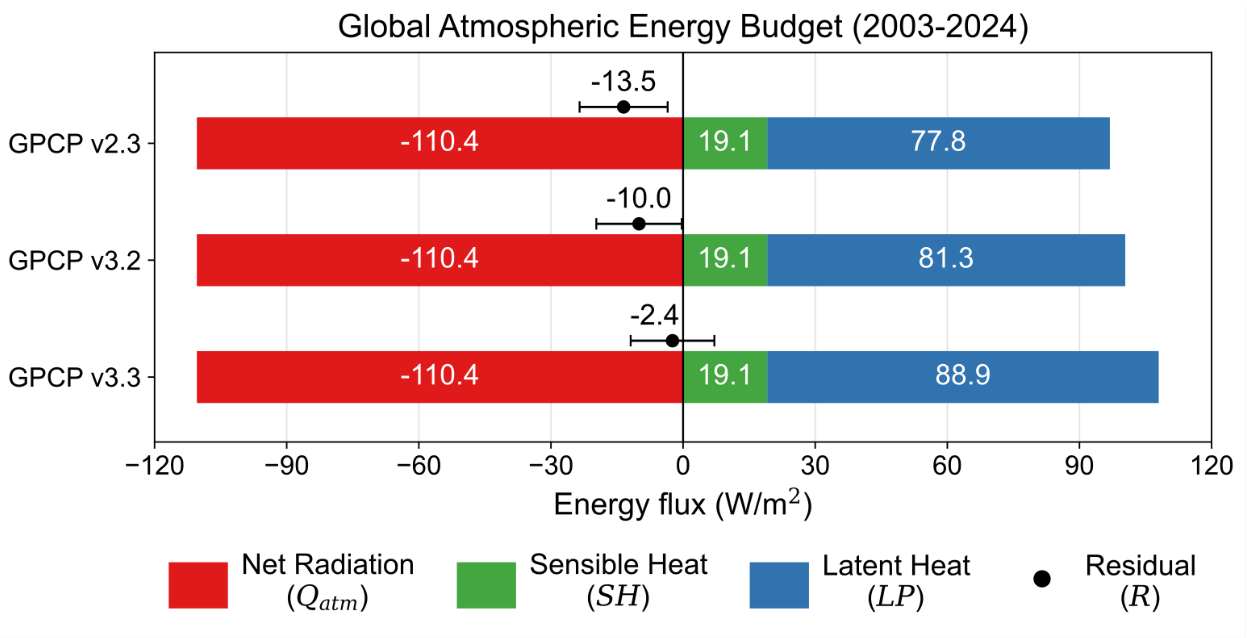

Figure 1. Global annual mean atmospheric energy budget closure across GPCP versions. Bar plot illustrating the components of the atmospheric energy balance: net atmospheric radiation (Q_{atm}), sensible heat (SH), and latent heat (LP). The residual ($R = Q_{atm} + SH + LP$) is shown for (top) GPCP v2.3, (middle) GPCP v3.2, and (bottom) GPCP v3.3. Error bars on the residual points are propagated uncertainty, calculated as root-sum-square of individual component errors. While Q_{atm} and SH remain constant, the increasing LP magnitudes in successive GPCP versions reduce the residual from -13.5 ± 10.0 W/m^2 (v2.3) to -2.4 ± 9.5 W/m^2 (v3.3), the latter achieving a 98% closure of the mean-state energy budget.

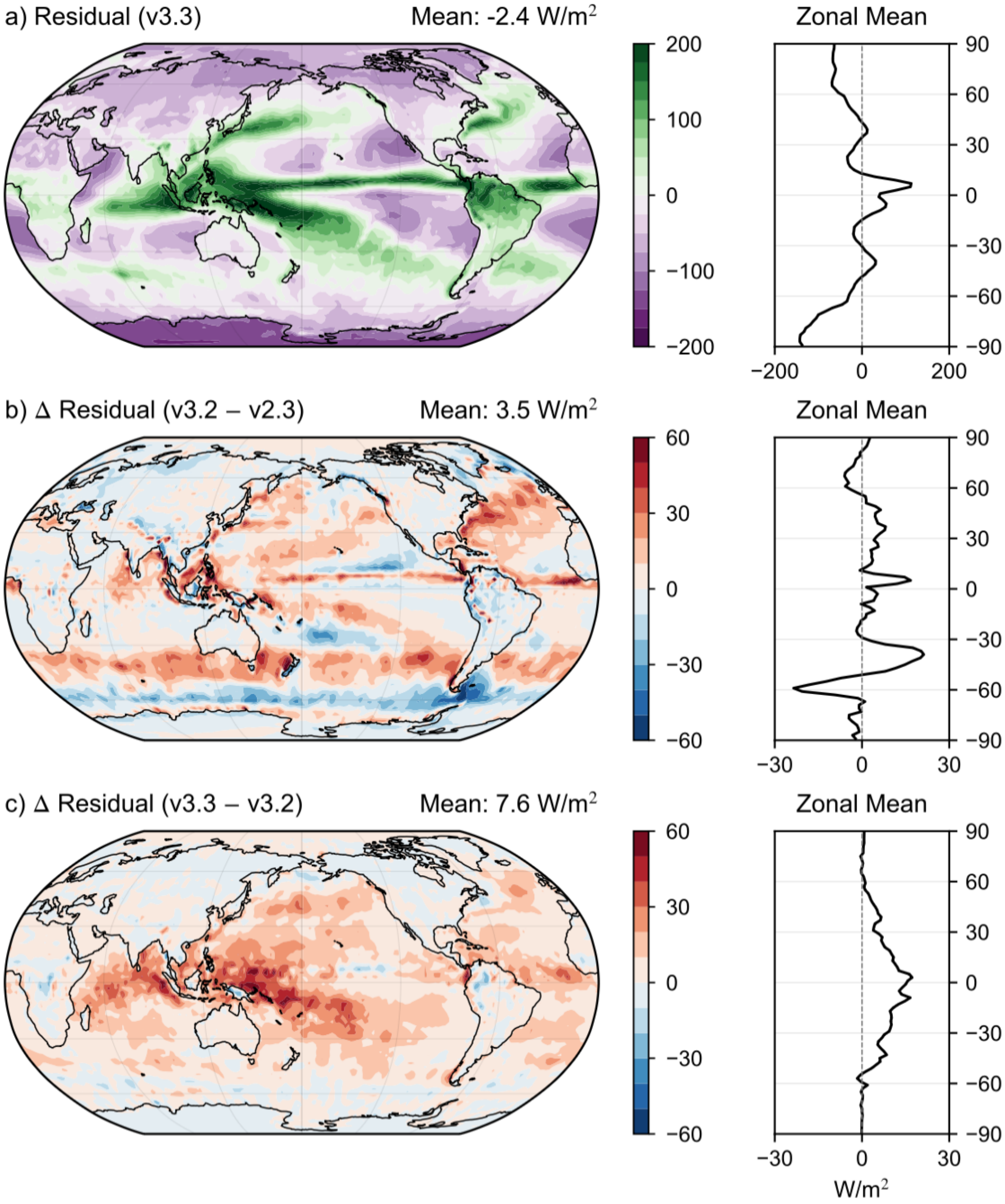

Figure 2. Global distribution and zonal mean of atmospheric energy budget residuals. (a) Mean atmospheric energy residual (W/m^2) calculated using CERES EBAF Ed4.2 (Net TOA and Surface), MERRA-2 (Sensible Heat Flux), and GPCP v3.3 (Latent Heat). (b) Difference in atmospheric residual resulting from the transition from GPCP v2.3 to v3.2. (c) Difference in atmospheric residual between GPCP v3.3 and v3.2. Zonal mean profiles (right column) correspond to each map, with latitude ranges from 90°S to 90°N. Area-weighted global means for each panel are indicated in the top-right of the map headers. All data are climatological means for the period January 2003 to April 2024.

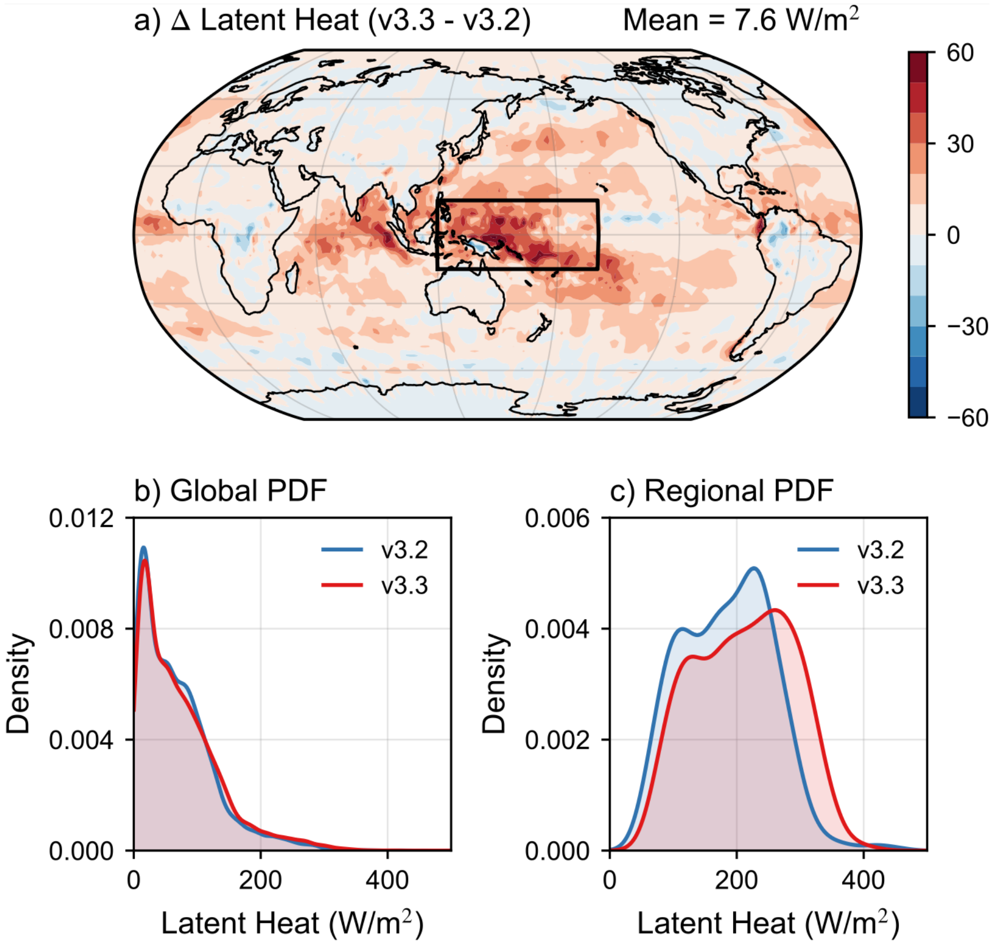

Figure 3. Spatial and statistical distribution of latent heat flux changes from GPCP v3.2 to v3.3. (a) Global distribution of the mean latent heat difference (v3.3 minus v3.2), highlighting a concentrated increase over the Tropical West Pacific (TWP; 120°E–160°W, 15°S–15°N). (b) Probability distribution functions (PDFs) of global latent heat for v3.2 (blue) and v3.3 (red), showing the shift in global mean state. (c) PDFs of regional latent heat over the TWP, illustrating a distinct rightward shift toward higher latent heat intensities in v3.3.

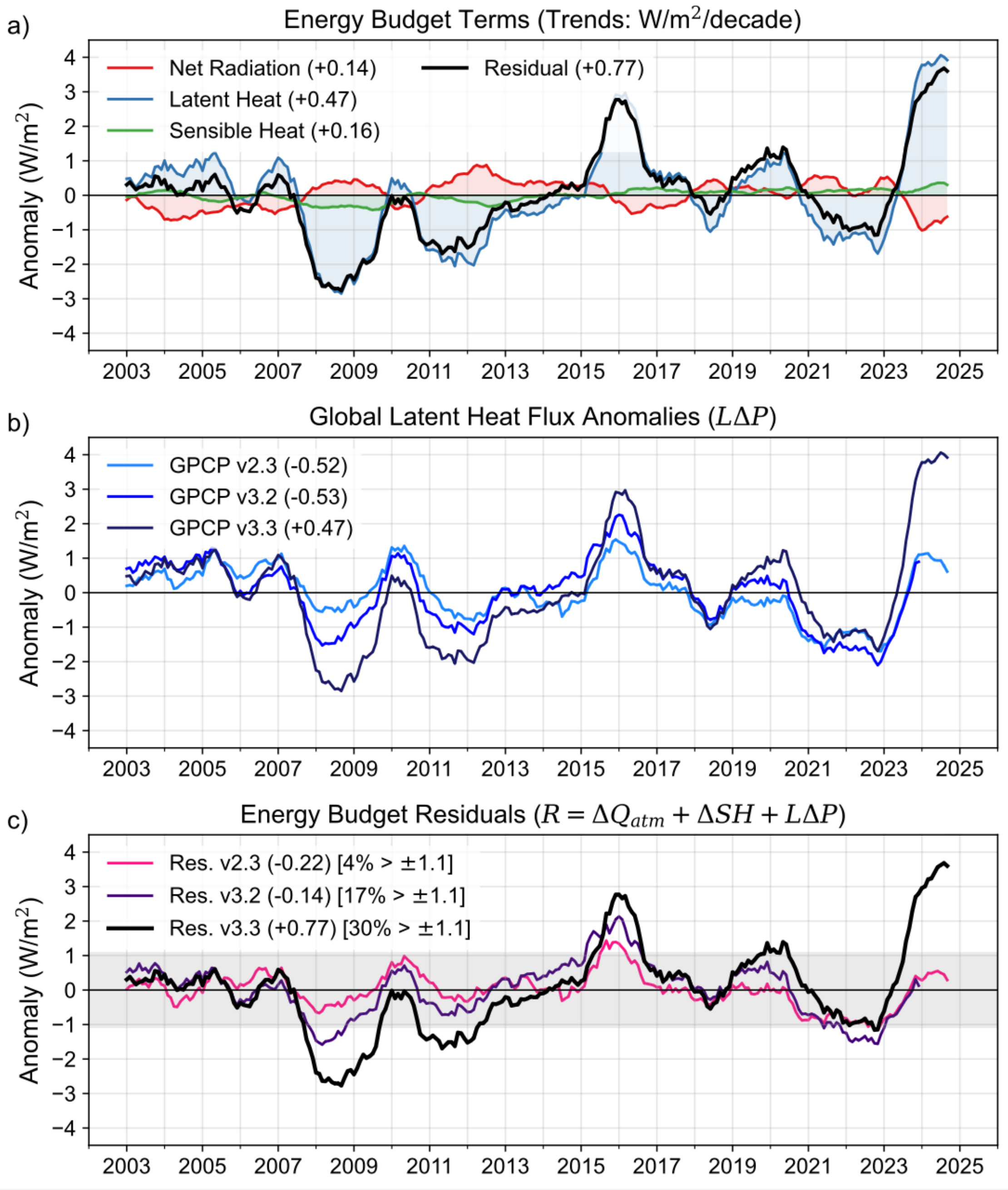

Figure 4. Interannual variability and the variability paradox in the atmospheric energy budget (2003–2024). (a) Time series of global energy budget anomalies (Q_{atm}, *LP*, *SH*, and *R*) using GPCP v3.3, where the residual (*R*) is primarily driven by latent heat fluctuations. (b) Comparison of *LP* anomalies across GPCP v2.3, v3.2, and v3.3, showing a progressive increase in interannual variance with each version update. (c) Total budget residuals for the three GPCP versions. The gray shaded area denotes a ±1.1 W/m^2 uncertainty window. The percentage of time steps falling outside this window increases from 4% (v2.3) to 30% (v3.3), illustrating the trade-off between mean-state closure and anomaly stability.

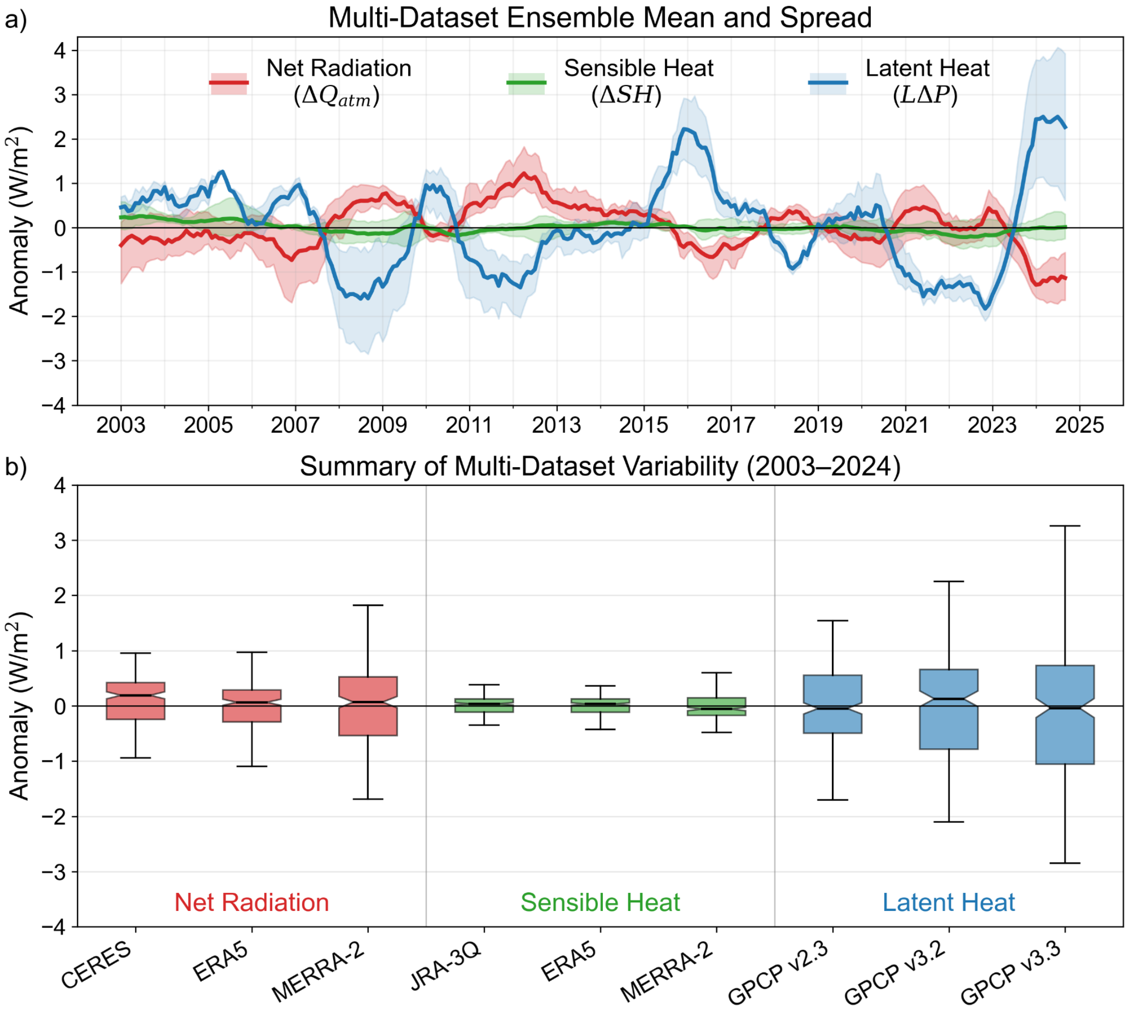

Figure 5. Global atmospheric energy flux anomalies and inter-dataset variability (2003–2024). (a) Multi-dataset ensemble monthly mean anomalies (W/m^2) for net radiation (ΔQ_{atm}, red), sensible heat (ΔSH, green), and latent heat ($L\Delta P$, blue). Solid lines represent the ensemble mean, while shaded envelopes denote the full range (min–max) across the constituent datasets (CERES, ERA5, MERRA-2, JRA-3Q, and GPCP versions). (b) Statistical summary of multi-dataset variability. Boxplots illustrate the distribution of anomalies for individual products over the study period. Boxes indicate the interquartile range (IQR), horizontal black lines denote the median, and whiskers extend to the full range of the data (0th to 100th percentiles). All anomalies are calculated relative to the 2003–2024 climatology.

References

Adler, R. F., Sapiano, M. R., Huffman, G. J., Wang, J. J., Gu, G., Behrangi, A. & Smith, E. (2018). The Global Precipitation Climatology Project (GPCP) monthly analysis (new version 2.3) and a review of 20 years of satellite heritage. *Remote Sensing*, 10(12), 1883. https://doi.org/10.3390/rs10121883

Allan, R. P., Liu, C., Loeb, N. G., Paolino, D. A., & Shin, D. W. (2014). Changes in global net radiative imbalance 1985–2012 bound by observations. *Nature Geoscience*, 7(3), 203-208. https://doi.org/10.1038/ngeo2088

Bolvin, D. T., Huffman, G. J., & Braithwaite, D. (2024). *Algorithm Theoretical Basis Document (ATBD) for the Global Precipitation Climatology Project (GPCP) Version 3.3*. NASA Goddard Space Flight Center.

Global Modeling and Assimilation Office (GMAO). (2015). *MERRA-2 instM_2d_asm_Nx: 2d, Monthly mean, Instantaneous, Analysis, State, Native resolution v5.12.4* [Data set]. Goddard Earth Sciences Data and Information Services Center (GES DISC). https://doi.org/10.5067/2E09B8UQZ7A6

Held, I. M. & Soden, B. J. (2006). Robust Responses of the Hydrological Cycle to Global Warming. *Journal of Climate*, 19(21), 5686-5699. https://doi.org/10.1175/JCLI3990.1

Hersbach, H., Bell, B., Berrisford, P., Hirahara, S., Horányi, A., Muñoz-Sabater, J., et al. (2020). The ERA5 global reanalysis. *Quarterly Journal of the Royal Meteorological Society*, 146(730), 1999-2049. https://doi.org/10.1002/qj.3803

Huffman, G. J., Bolvin, D. T., Braithwaite, D., Hsu, K., Joyce, R., Kidd, C., et al. (2020). *Integrated Multi-satellitE Retrievals for GPM (IMERG) Final Run Release 06 V06B Notes*. NASA Goddard Space Flight Center.

Huffman, G. J., Bolvin, D. T., Braithwaite, D., Hsu, K., Joyce, R., Kidd, C., et al. (2023). *Global Precipitation Climatology Project (GPCP) Monthly Analysis Product, Version 3.2* [Data set]. NASA Goddard Earth Sciences Data and Information Services Center (GES DISC). https://doi.org/10.5067/MEASURES/GPCP/DATA303

Huffman, G. J., Bolvin, D. T., Braithwaite, D., Hsu, K., Joyce, R., Kidd, C., et al. (2024). *Global Precipitation Climatology Project (GPCP) Monthly Analysis Product, Version 3.3* [Data set]. NASA Goddard Earth Sciences Data and Information Services Center (GES DISC). https://doi.org/10.5067/MEASURES/GPCP/DATA303

Jakob, C., Singh, M. S., & Jungandreas, L. (2019). Radiative convective equilibrium and organized convection: An observational perspective. *Geophysical Research Letters*, *46*(9), 5009–5017. https://doi.org/10.1029/2019GL082442

Jones, P. W. (1999). First-and second-order conservative remapping schemes for grids in spherical coordinates. *Monthly Weather Review*, 127(9), 2204-2210. https://doi.org/10.1175/1520-0493(1999)127<2204:FASOCR>2.0.CO;2

Kato, S., Thorsen, T. J., Rose, F. G., Loeb, N. G., Ham, S. H., Rutan, D. A., ... & Allan, R. P. (2025). Satellite observed trends of global mean net atmospheric shortwave and longwave irradiances and diabatic heating by precipitation. *Science Advances*, 11(42), eadz1292. https://doi.org/10.1126/sciadv.adz1292

Kramer, R. J., Matus, A. V., Soden, B. J., & L'Ecuyer, T. S. (2019). Observation-based radiative kernels from CloudSat/CALIPSO. *Journal of Geophysical Research: Atmospheres*, 124(10), 5431–5444. https://doi.org/10.1029/2018JD029918

L’Ecuyer, T. S., Beaudoing, H. K., Rodell, M., Olson, W., Lin, B., Adler, S., ... & Zhou, T. (2015). The observed state of the energy budget in the early twenty-first century. *Journal of Climate*, 28(21), 8319–8346. https://doi.org/10.1175/JCLI-D-14-00556.1

Loeb, N. G., Doelling, D. R., Wang, H., Su, W., Nguyen, C., Corbett, J. G., ... & Meyer, K. (2018). Clouds and the Earth's Radiant Energy System (CERES) Energy Balanced and Filled (EBAF) Top-of-Atmosphere (TOA) Edition-4.0 Data Product. *Journal of Climate*, 31(2), 895-918. https://doi.org/10.1175/JCLI-D-17-0208.1

Loeb, N. G., Doelling, D. R., Kato, S., Su, W., Mlynczak, P. E., & Wilkins, J. C. (2023). Continuity in top-of-atmosphere Earth radiation budget observations. *Journal of Climate*, 36(15), 5121–5133. https://doi.org/10.1175/JCLI-D-22-0853.1

Matus, A. V., & L’Ecuyer, T. S. (2017). The role of cloud phase in Earth's radiation budget. *Journal of Geophysical Research: Atmospheres*, 122(5), 2559-2578. https://doi.org/10.1002/2016JD025951

NASA/LARC/ASDC. (2023). *CERES EBAF-TOA and EBAF-Surface Edition 4.2.1* [Data set]. NASA Langley Atmospheric Science Data Center. https://doi.org/10.5067/TERRA+AQUA-DATASET/CERES/EBAF_L3-4.2

O'Gorman, P. A., Allan, R. P., Byrne, M. P., & Previdi, M. (2012). Energetic constraints on precipitation under climate change. *Surveys in Geophysics*, 33, 585-608. https://doi.org/10.1007/s10712-011-9159-6

Oreopoulos, L., Cho, N., & Lee, D. (2025). The role of Earth’s major cloud systems in the hemispheric albedo symmetry. *Geophysical Research Letters*, *51*(2), e2023GL105953. https://doi.org/10.1029/2023GL105953

Sherwood, S. C., Bony, S., & Dufresne, J. L. (2015). Spread in model climate sensitivity traced to atmospheric convective mixing. *Nature*, 505(7481), 37-42. https://doi.org/10.1038/nature12829

Stephens, G. L., Li, J., Wild, M., Clayson, C. A., Loeb, N. G., Kato, S., ... & Andrews, T. (2012). An update on Earth's energy balance in light of the latest global observations. *Nature Geoscience*, 5(10), 691-696. https://doi.org/10.1038/ngeo1580

Sun-Mack, S., Minnis, P., Chen, Y., Gibson, S., Yi, Y., Arduini, R. F., ... & Smith, W. L. (2018). CERES Edition 4 cloud property retrievals over snow and ice surfaces from MODIS and VIIRS. *IEEE Transactions on Geoscience and Remote Sensing*, 56(10), 6010-6040.